water

MDPI

Article

Prediction and Management of the Groundwater Environmental Pollution Impact in Anning Refinery in Southern China

Xiaoqi Fang [1], Shiyao Tang [1,*], Zhenru Niu [2] and Juntao Tong [1]

[1] No.290 Research Institute of Nuclear Industry, Shaoguan 512026, China; fxqcnnc@126.com (X.F.); 15015062475@163.com (J.T.)
[2] Tianjin North China Geological Exploration General Institute, Tianjin 300170, China; niuzhenru@126.com
* Correspondence: yycnnc@126.com; Tel.: +86-138-0281-9720

Abstract: Anning Refinery, a large-scale joint venture in southern China, possesses significant potential in regard to polluting local groundwater environments due to its extensive petroleum raw materials. This study aims to mitigate the substantial risks associated with oil spills and prevent consequential groundwater pollution by developing a robust groundwater flow model using the MODFLOW module in GMS software that aligns closely with natural and pumping test conditions. Furthermore, by integrating the MT3DMS model, a groundwater solute transport model is constructed and calibrated using sodium chloride tracer dispersion data. Notably, the wax hydrocracking unit and aviation coal finished product tank area are identified as key pollution sources warranting attention. By considering local constraints such as karst collapse, ground subsidence, and single-well water output capacity, the study introduces a tailored groundwater pollution management model. The research simulates various scenarios of petroleum pollutant migration in groundwater and proposes multi-objective emergency response optimization plans. In Scenario 1, simulations show that petroleum pollutants migrate within the unconfined aquifer and enter the karst aquifer as low-concentration plumes over an extended period. Detection of these plumes in karst water monitoring wells indicates upstream unconfined aquifer contamination at higher concentrations, necessitating immediate activation of the nearest monitoring or emergency wells in both layers. Conversely, in Scenario 2, pollutants reside briefly in the unconfined aquifer before entering the karst aquifer at relatively higher concentrations. Here, low-efficiency pollutant discharge through unconfined aquifer monitoring wells prompts the activation of nearby karst aquifer monitoring or emergency wells for effective pollution control. This model underscores the necessity for proactive monitoring and validates the efficacy of coupled numerical modeling in understanding pollutant behavior, offering valuable insights into pollution control scenario assessments. In summary, the study emphasizes the importance of targeted monitoring and emergency protocols, demonstrating the benefits of integrated modeling approaches in industrial areas prone to pollution risks, and provides critical theoretical and practical guidance for groundwater protection and pollution management, offering transferable insights for similar industrial settings worldwide.

Keywords: groundwater flow numerical simulation; solute transport model; groundwater pollution prevention and control management plan; petroleum pollutants; Yunnan Anning Refinery

Citation: Fang, X.; Tang, S.; Niu, Z.; Tong, J. Prediction and Management of the Groundwater Environmental Pollution Impact in Anning Refinery in Southern China. *Water* **2024**, *16*, 2713. https://doi.org/10.3390/w16192713

Academic Editors: Constantinos V. Chrysikopoulos and Dimitrios E. Alexakis

Received: 2 July 2024
Revised: 21 August 2024
Accepted: 2 September 2024
Published: 24 September 2024

1. Introduction

With the continuous advancement of global industrialization and urbanization, environmental pollution issues are becoming increasingly severe, with groundwater pollution being particularly prominent [1]. As an important water resource, groundwater is widely used in agricultural irrigation and industrial water supply, and it directly impacts the safety of human drinking water [2]. However, due to the hidden and complex nature of groundwater flow, its pollution control is challenging, with a wide diffusion range, long recovery period, and high treatment costs, making it a major problem in environmental

protection [3]. In recent years, groundwater pollution has garnered widespread attention and significant concern in countries such as the United States [4,5], Australia [6], Japan [7], and China [8,9]. Groundwater pollution not only affects water quality but also impacts surface water and the ecological environment through the hydrological cycle, further threatening human health and the stability of ecosystems [10]. To address this issue, many scholars have conducted extensive research on groundwater pollution prevention and control, aiming to reveal the mechanisms of groundwater pollution, its migration patterns, and effective prevention and control methods [11], focusing mainly on pollution source identification [12], pollutant migration mechanisms [13], pollution prevention and control technologies [14], and numerical simulations [15].

Identifying pollution sources is the first step in groundwater pollution prevention and control. Identification techniques mainly involve isotope tracing technology [16,17], multivariate statistical analysis [18], and geochemical models [19] to precisely locate groundwater pollution sources. Matiatos used a Bayesian isotope mixing model (SIAR) and multivariate statistical analysis of groundwater hydrochemical data to estimate the relative contributions of different nitrate sources and identify the dominant factors controlling nitrate levels in the area's groundwater, revealing that urban and industrial waste in the basin are the main causes of groundwater nitrate pollution in these regions [18]. Wu and colleagues successfully identified nitrate pollution sources in the groundwater of a critical red soil observation station in China using dual nitrogen isotope tracing technology [20]. Naderi and colleagues used chemical isotope analysis, geochemical models, health risk assessments, and multivariate statistical methods to investigate the pollution and sources of fluoride in cold and hot spring groundwater, and they also assessed the water pollution issues and health risks associated with fluoride [21]. Shao and colleagues used electrical resistivity tomography (ERT) data to design vertical barrier walls to prevent further migration of pollutants. Their results showed that pollutants mainly accumulated in fracture zones around the landfill, with the main migration channels being the densely faulted zones on the north and south sides of the landfill, and the migration direction was consistent with groundwater flow [22]. Meanwhile, understanding the migration mechanisms of pollutants in groundwater is key to formulating effective treatment plans. Organic pollutants in groundwater exhibit significant differences in migration speed and diffusion range under different geological conditions, posing challenges to the accuracy of pollution prediction models. Some studies have also focused on the impact of non-linear adsorption and the degradation reactions of pollutants on the migration process [23,24]. Guo and Brusseau pointed out that PAT technology can effectively control pollutant diffusion and provide insights into the closure potential of large, complex contaminated sites, offering references for site management performance indicators. However, long-term use may lead to aquifer structure damage [25].

Currently, numerical simulation is an important tool for studying the migration of groundwater pollutants. Various simulation software such as MODFLOW [26,27], FEMWATER [28,29], and HYDRUS [30–33] have been successfully developed to simulate pollutant migration under different geological conditions. Zhou and colleagues designed four future long-term climate change scenarios for the Alxa region in Inner Mongolia, China, and accurately simulated groundwater flow changes using GMS [34]. To capture the heterogeneity and morphology of pollutants, Tabelin and colleagues combined geochemical auditing with numerical simulation, successfully predicting the flow paths and migration of acidic mine drainage from a legacy mine in Japan [35]. Vu and Ni used the index overlay method (DRASTIC method) and a physics-based numerical model (MODFLOW model) to predict groundwater sustainability and pollution migration under different scenarios, showing that coupled groundwater flow and solute transport models can more accurately predict pollutant migration paths and concentration distributions [36]. Currently, the GMS groundwater flow numerical model with the MT3DMS solute transport model is widely used in groundwater environmental research due to its fast computation, simple operation,

and ability to accurately simulate the migration process of pollutants in groundwater bodies [37–39].

Groundwater pollutants mainly include heavy metal pollutants [40], organic pollutants [41], and petroleum pollutants [42]. These pollutants penetrate and diffuse into the groundwater system, forming pollution plumes that spread with groundwater flow, gradually expanding the contamination area [43–45]. The groundwater pollution problem is particularly severe in areas with concentrated petrochemical enterprises. As an important part of petrochemical enterprises, refineries produce pollutants during production that, once leaked, pose a serious threat to the groundwater environment [46]. Based on this, this study takes the Yunnan Anning Refinery in China as an example, coupling the GMS groundwater flow numerical model with the MT3DMS solute transport model to develop a groundwater pollution prevention and control management model. It reveals the groundwater flow and petroleum pollutant migration patterns in the refinery area, simulates the diffusion paths and concentration changes in petroleum pollutants under different scenarios, and further proposes a multi-objective emergency optimization removal plan for pollutants, aiming to provide a scientific theoretical basis for protecting local groundwater resources.

2. Overview of the Study Area and Data Sources

2.1. Overview of the Study Area

The construction site of the joint venture refinery, with a capacity of ten million tons, is located in Anning City, Yunnan Province, at geographic coordinates 102°21′–102°23′ E and 24°54′–24°55′ N. The general terrain of the study area is high in the south and low in the north, belonging to the mid-mountain to low-mountain type. The terrain slope ranges from 25° to 35°, with mountain elevations between 2200 and 2500 m and relative height differences generally less than 500 m. The landform is mainly characterized by shallow-cut, structurally eroded low-mid mountain terrain, with depositional landforms developing along riverbanks and intermountain basins. The main exposed strata in the study area include the Cambrian Yuqucun Formation, the Cambrian Qiongzhusi Formation, the Devonian Haikou Formation, the Devonian Zaige Formation, and the Quaternary system (Figure 1). Among these, the Quaternary unconfined aquifer is widely covered, generally thicker in the west and thinner in the east, with some areas in the central part being relatively thin. The groundwater mainly includes three types: carbonate rock fissure and karst water, bedrock fissure water, and loose rock pore water. The study area's river systems belong to the Honghe River Basin and the Jinsha River Basin, with the western part in the Honghe River Basin and the eastern part in the Tanglangchuan River Basin, both of which are part of the Jinsha River system. The Unnamed River is the only river flowing through the refinery project area and is a seasonal stream. The local area is situated in a low-latitude subtropical highland monsoon climate zone and characterized by warm winters, cool summers, and dry conditions with little rainfall. The average annual temperature is 15.4 °C, with an average annual rainfall of 898.7 mm, 60% of which mainly occurs from July to September. The average annual evaporation is as high as 1994.3 mm.

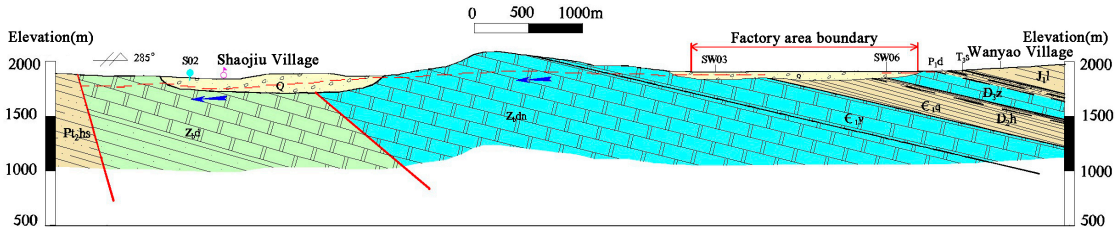

Figure 1. Hydrogeological profile.

2.2. Data Sources

The hydrogeological data in the study area are mainly provided by the First Hydrogeological and Engineering Geological Team of the Yunnan Bureau of Geology and Mineral

Resources and the Geotechnical Engineering Company of China Petroleum Engineering Construction Corporation. The meteorological data mainly come from the Hydrological and Water Resources Monitoring Center of Yunnan Province and the National Meteorological Science Data Sharing Service Platform. Hydrogeological parameters, groundwater levels, tracer concentrations, and other data are from the special geophysical survey and karst exploration report of the Anning Refinery in Yunnan. There are a total of 18 groundwater real-time monitoring wells in the factory area, mainly monitoring changes in water levels in pore water and karst water. There are also 10 emergency pollution control pumping wells which are used to intercept and pump water to prevent pollutants from migrating downward. At the same time, the extracted contaminated groundwater is transported to the surface treatment facilities for treatment to remove dissolved pollutants in the water. The distribution of monitoring wells and pumping wells is shown in Figure 2.

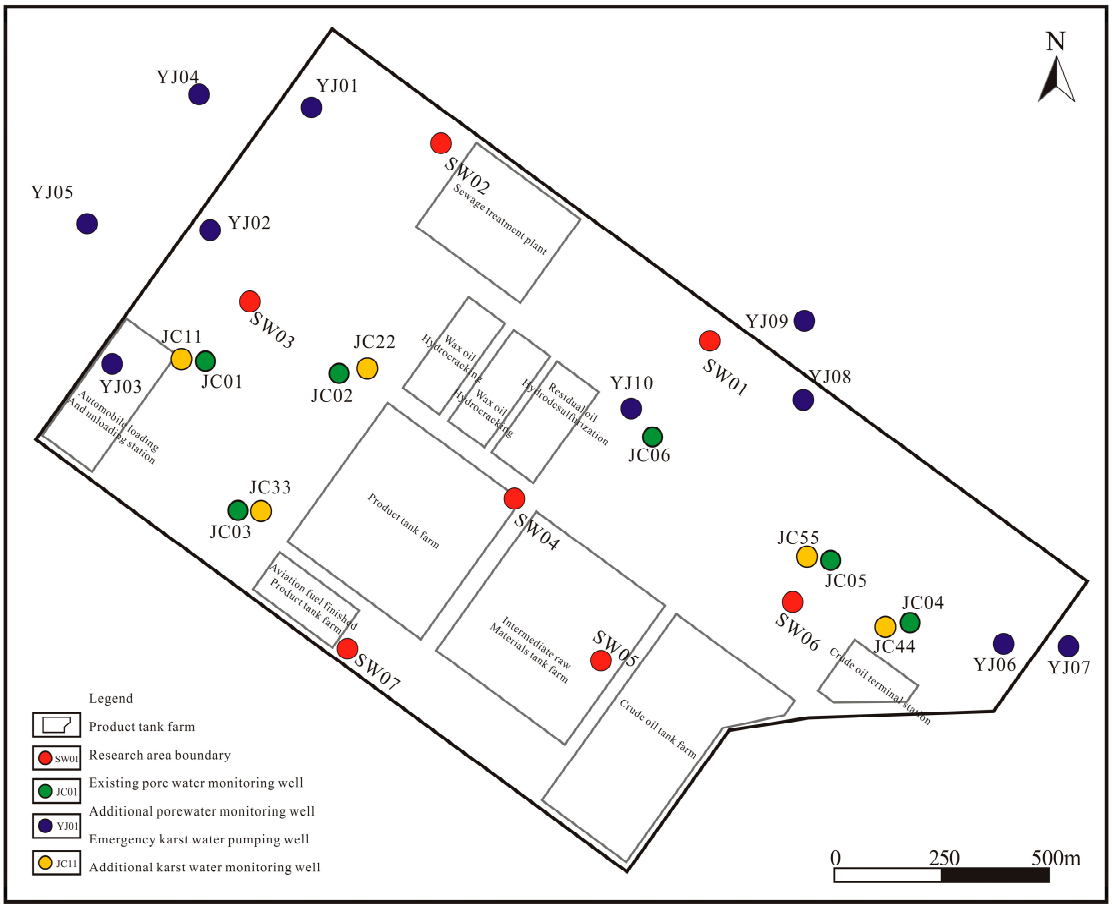

Figure 2. Distribution map of groundwater monitoring points in the refinery area.

3. Groundwater Flow Numerical Simulation

The unconfined aquifer of the fourth series is widely distributed in the factory area, mainly composed of backfill, floodplain deposits, lake facies deposits, and residual slope deposits, with a thickness of about 14–35.5 m. When pollutants leak, the unconfined aquifer of the fourth series will be the first to be contaminated. After pollutants enter the sand and gravel layer, the migration speed of pollutants accelerates, spreading to surrounding areas downstream and infiltrating downward into the bedrock. Firstly, we develop a numerical model of groundwater flow in the shallow unconfined aquifer of the factory area, further develop a water quality model for the factory area, and then couple the numerical model of groundwater flow with the water quality model to form a pollution prevention and control management model for the shallow unconfined aquifer of the factory area.

3.1. Development of Hydrogeological Conceptual Model

3.1.1. Generalization of Aquifer (Aquiclude) Structure

The unconfined aquifer of the fourth series in the factory area is mainly composed of backfill, floodplain deposits, and residual slope deposits. The lithological characteristics are divided into four layers from top to bottom. The first layer is mainly filled with soil, mainly composed of limestone, sandstone debris, and loamy clay. This layer is discontinuously distributed, with a thickness of 0.20 to 5.40 m and a bottom elevation of 1888.49 to 1920.54 m. The second layer is loamy clay, containing a small amount of silica, limestone gravel, and manganese oxide nodules and spots. The thickness is 0.20 to 15.90 m, and the bottom elevation is 1875.80 to 1934.83 m. The third layer is composed of angular gravelly loamy clay, mainly loamy clay, with an angular gravel content of 5% to 30% and a particle size of 3 to 50 mm. The components of the gravel are mainly limestone, phosphatic sandstone, and a small amount of siliceous rock. The thickness is 0.50 to 25.50 m and the bottom elevation is 1857.18 to 1911.78 m. The fourth layer is residual soil, mainly loamy clay and locally red clay, which comprises residual slope deposits of various rocks after weathering, mainly composed of feldspar, mica, limestone, and other carbonate minerals, with embedded quartz particles. The thickness is 0.60 to 16.80 m and the bottom elevation is 1853.14 to 1914.15 m.

The MODFLOW module in GMS software was used to develop a numerical model of groundwater in the factory area using the conceptual model method. First, the actual hydrogeological conditions were generalized to develop a hydrogeological conceptual model. Based on the lithological characteristics of the unconfined aquifer, the layers containing clay, coarse gravel, sand, and gravel layers were generalized into aquifers, while layers containing plain soil, cultivated soil, loamy clay, gravelly clay, gravelly loamy clay, residual soil, clayey soil with sand, and organic matter were generalized into relatively impermeable layers. After the factory area was leveled, the artificially filled soil in the low-lying areas was compacted, and the artificially filled soil was also generalized into aquifers. The generalized model of the unconfined aquifer in the study area is shown in Figure 3. The model is generalized into three layers: the first layer is filled with soil and clay, forming a continuous aquiclude; the second layer is mainly clay, with some sand and gravel; the third layer is mainly sand and gravel, with some residual soil. The sand and gravel aquifer is a discontinuous aquifer distributed in the second and third layers of the model. In some areas, the aquifer directly contacts the underlying bedrock.

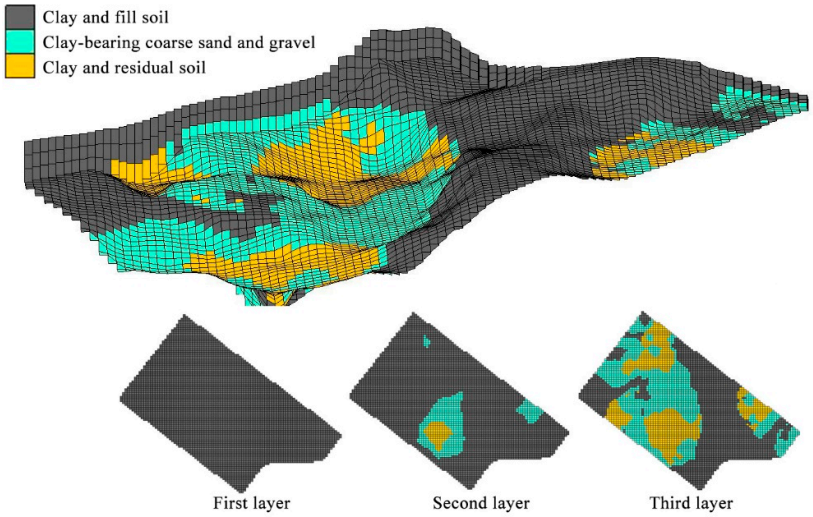

Figure 3. Conceptual model of the unconsolidated layer.

3.1.2. Conceptualization of Boundary Conditions

The simulated area of this model is the unconfined aquifer of the plant area. It is underlain by the Zhaige Formation, Haikou Formation, Qiongzhushi Formation, and Yuhucun

Formation bedrock of the plant area. The Haikou and Qiongzhushi Formations have poor permeability while the Zhaige and Yuhucun Formations have developed karst features and are hydraulically connected to the overlying unconsolidated layer, allowing the fourth series unconsolidated layer to be divided into a relatively independent hydrogeological unit (as shown in Figure 1). The aquifer consists of sand and gravel layers of the fourth series, with the overlying clay layer acting as a relatively impermeable layer. The groundwater is slightly under pressure. The main groundwater recharge methods are atmospheric precipitation and lateral flow recharge from the karst water of the Zhaige Formation in the east. Overall, the flow is from southeast to northwest, with the main discharge methods being atmospheric evaporation and discharge to adjacent areas. Vertically, the pore water in the unconsolidated layer of the plant area and the karst fissure water are hydraulically connected through a weakly permeable layer between them, and in some areas, the aquifer directly discharges into the karst aquifer.

In the northeastern and southeastern parts of the plant area, it is adjacent to the Qiongzhushi Formation shale, siltstone, and sandstone, with weak hydraulic connections which are conceptualized as impermeable boundaries; in the east, it is adjacent to the Zhaige Formation dolomite, and, based on borehole observations, the Zhaige Formation has a higher water head (YJ07 is an artesian well) which recharges the unconsolidated layer, conceptualized as a specified head boundary; in the northwest, the fourth series unconsolidated layer is in contact with the underlying Yuhucun Formation dolomite, where the groundwater level is lower than that of the unconsolidated layer, so the unconsolidated layer recharges the Yuhucun Formation; in the southwest, there is an exchange of water between the unconsolidated layers and the plant area unconsolidated layer, and the water level in the boreholes at the plant boundary is known (Table 1), so it can be conceptualized as a mixed boundary. The conceptual model diagram after conceptualization is shown in Figure 4a.

Table 1. Water levels of boreholes at the southwestern and northwestern boundaries of the plant area.

Borehole No.	Water Level	Borehole No.	Water Level
ZK151	1885.34	ZK20	1907.59
ZK209	1888.02	ZK24	1909.42
ZK262	1885.17	ZK30	1908.26
ZK298	1888.23	ZK150	1908.24
ZK352	1897.42	ZK208	1913.94
ZK12	1886.74	JC44	1909.567
ZK16	1912.73	YJ06	1912.71

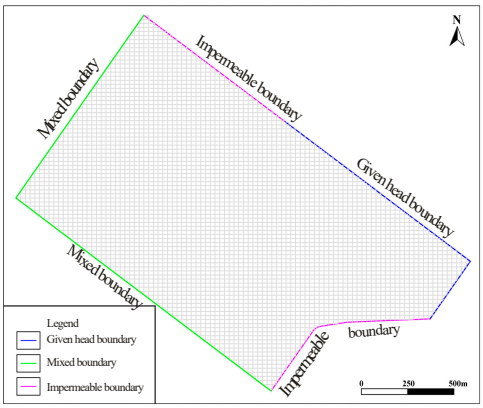

(**a**) Conceptual model and grid partitioning of the unconfined aquifer in the factory area

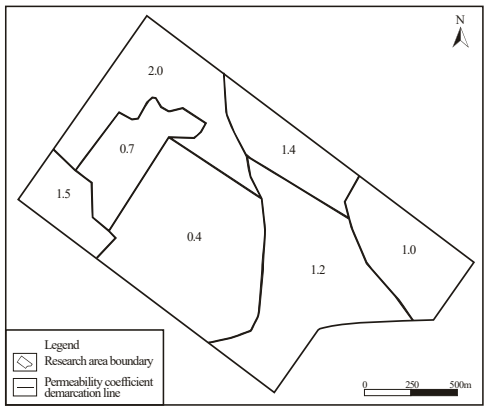

(**b**) Permeability zoning map of the third layer (unit: m/d)

Figure 4. Conceptualization of Boundary Conditions.

3.2. Mathematical Model Development

By analyzing borehole data and hydrogeological survey data, the aquifer in the study area is conceptualized as a heterogeneous, isotropic, spatially multi-layered, and stable groundwater flow system. The groundwater system in this area consists of confined and unconfined water, so the following mathematical models are selected to describe it:

$$\begin{cases} \frac{\partial}{\partial x}\left(K_{xx}\frac{\partial H}{\partial x}\right)+\frac{\partial}{\partial y}\left(K_{yy}\frac{\partial H}{\partial y}\right)+W=0 \ \ (x,y)\in\Omega \\ \mathrm{K}\frac{\partial H}{\partial n}\Big|S_2=q_1(x,y,t) \ \ (x,y)\in S_2 \\ \frac{\partial H}{\partial n}+\alpha H=\beta \ \ \alpha,\beta\text{are known functions;} \\ H(x,y,t)|t=0=H_0(x,y) \ \ (x,y)\in D \end{cases} \quad (1)$$

In Equation (1):

Ω represents the groundwater seepage area;

S_1 is the first type boundary of the model;

S_2 is the second type boundary of the model;

k_{xx}, k_{yy} and k_{zz} represent the permeability coefficients in the x, y, and z directions (m/s), respectively;

w represents the source–sink term, including the precipitation infiltration supply, evaporation, pumping rate of wells, and discharge rate of springs (m^3/s);

$H_0(x, y, z)$ is the groundwater head function at the first type boundary (m);

$q(x, y, z)$ is the unit area flow rate function at the second type boundary (m^3/s);

T_{xx}, T_{yy}, and T_{zz}, respectively, represent the average transmissivity during the management period [$L^2\Gamma^{-1}$];

Ss is the specific yield, unit m^{-1}.

3.3. Numerical Model Development

3.3.1. Grid Partitioning

The study area covers an area of 2.513 km^2 and the hydrogeological unit is a confined-aquifer system. Based on field drilling data, geological entities are developed and imported into the MODFLOW software. The grid is partitioned into 100 × 100 × 3 cells (Figure 4a).

3.3.2. Source and Sink Terms

Recharge: Groundwater mainly receives recharge from precipitation. According to statistical studies, the average annual precipitation in the study area is 1191 mm/a and the local coefficient of precipitation infiltration is 0.0185. Therefore, the recharge of groundwater from precipitation can be calculated as 0.00006 m/d.

Discharge: Groundwater in this area mainly laterally discharges to the northwest into the aquifer of the Yuhu Village Formation.

3.3.3. Hydrogeological Parameters

Permeability: The determination of permeability mainly relies on calculated values from single-well pumping tests in the factory area combined with regional data for model parameter adjustment. Permeability ranges from 0.101 to 1.491, affecting the radii of influence from 4.603 to 21.392 m. The estimated single-well pumping rates range from 1.296 to 6.307 m^3/d. The permeability is uniformly set at 0.008 m/d for backfill soil and clay and at 0.01 m/d for residual soil and clay. The second layer of the model has only local occurrences of sand and gravel lenses, with a permeability of 1.0 m/d for these lenses. As the aquifer mainly occurs in the third layer of the model, parameter zoning and fitting were performed for this layer (Figure 4b).

Effective Porosity: Based on empirical values, the effective porosity is set at 0.12.

Specific Yield: Based on empirical values, the specific yield for clay and backfill soil is set at 0.05, for gravel and clayey coarse sand at 0.17, and for clay and residual soil at 0.07.

3.4. Model Calibration and Validation

In the simulation area, the initial water level of the aquifer revealed by boreholes can be used as one of the model validation bases (Table 2), with a borehole water level observation error set at 2.0 m. In MODFLOW, there is a relationship between the observed borehole data and the software's simulated data. If the difference between the observed and calculated values is within the verification confidence interval, the error bar will be displayed in green. If it exceeds the verification confidence interval but is less than 200%, the error bar will be displayed in yellow. If it exceeds 200%, the error bar will be displayed in red, as shown in Figure 5.

Table 2. Summary of steady-state flow model fitting (unit: m).

Borehole No.	Measured Water Level	Calculated Water Level	Absolute Error
JC01	1904.172	1902.44	1.732
JC02	1904.544	1904.23	0.314
JC03	1905.41	1903.82	1.59
JC04	1910.526	1911.96	1.434
JC05	1908.166	1911.12	2.954
JC06	1906.352	1908.53	2.178
YJ10	1905.751	1907.79	2.039

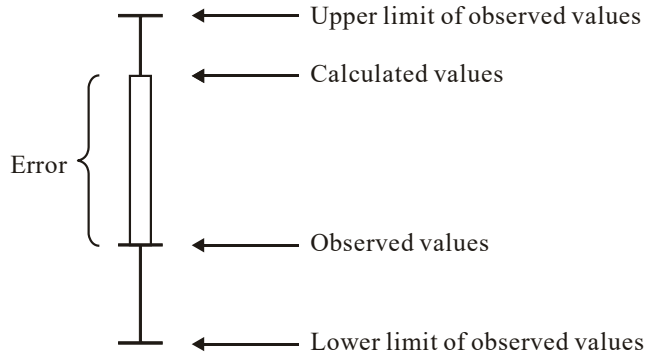

Figure 5. Error bar illustration.

The software simulation results are shown in Figure 6, where the calculated water levels at each observation well are within the set error range.

In summary, the calculated water levels fit well with the actual observed water levels, indicating a good agreement between the model and the reality. According to the model, the groundwater flow field generally flows from southeast to northwest under natural conditions.

In this numerical simulation work, it was considered that the pumping test assumed the aquifer to be uniformly distributed, but, in reality, the aquifer is non-uniformly distributed. When using hydrogeological parameters, the parameters of the study area were appropriately divided and assigned values based on the actual situation of the pumping test, and the initial model's parameter zoning was verified based on the actual measured water level data of the pumping test. After verification, if the water levels of each layer measured in the pumping test match well with the calculated water levels corresponding to the model, it indicates that the hydrogeological parameters used in the model can reflect the actual hydrogeological conditions of the study area, and this can be used to develop an optimized management model for the study area. Based on the initial model, single-hole pumping tests were used to validate the numerical simulation. The pumping rates of SW02 and SW04 were 6.307 m^3/d and 5.011 m^3/d, respectively. The water level of SW04 fitted well with the actual water level, with an error of 2.9 m.

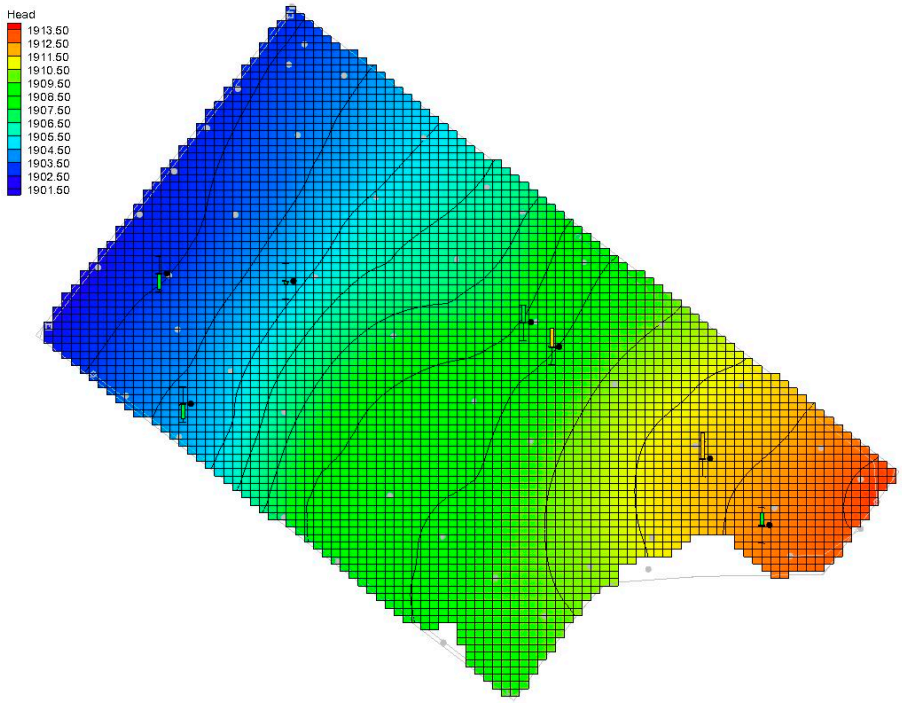

Figure 6. Natural field fitting graph.

4. Prediction of Groundwater Environmental Pollution Impact

4.1. Construction of Groundwater Solute Transport Model

Due to the poor hydraulic conductivity and permeability of the clay layer, the movement of pollutants through these areas is relatively slow, resulting in a minor impact on groundwater infiltration. Considering the occurrence of risks such as equipment, pipeline, rupture, and failure of the impermeable layer in the factory area, it is believed that pollutants will primarily enter the unconfined aquifer under this risk scenario, and the impact of pollutants on the unconfined aquifer is predicted. Based on the current impermeable measures, the potential leakage risks during the long-term production operation of the project are analyzed. These leakage areas mainly include the aviation coal finished tank area, wax oil hydrocracking unit, sewage treatment plant, automobile loading and unloading station, railway loading and unloading station, crude oil tank area, intermediate raw material tank area, product tank area, etc. According to this report, it is known that the oily wastewater in this project has the most significant impact on the groundwater environment. Therefore, the characteristic factor selected for this prediction evaluation is petroleum pollutants.

Considering the structure and distribution of the unconfined aquifer, the locations of the wax oil hydrocracking unit and the aviation coal finished tank area are directly above the karst aquifer in the loose aquifer layer without residual soil or clay to block them. In the event of a leak, pollutants would penetrate the unconfined aquifer and enter the karst aquifer, causing groundwater pollution. Therefore, the wax oil hydrocracking unit and the aviation coal finished tank area are selected as two potential pollution sources for predicting the transport of pollutants in the unconfined aquifer. The pollution sources are abstracted as continuous point sources, and once a pollution plume is detected at any monitoring well, the pollution source is cut off. The leakage source concentration is 500 mg/L, and physical and chemical reactions such as adsorption and degradation are not considered.

Solute transport is based on the water flow model, so the generalization of the water quality model should match the conceptual water flow model being developed. Parameters, initial conditions, and boundary conditions of the aquifer are input into the water quality model. By using the MODFLOW software, the water flow and water quality models are jointly run to obtain the migration results of the petroleum pollutants in the pore water.

Under natural conditions, pollutants generally migrate towards the northwest. The initial concentration of pollutants in groundwater is simulated to be 500 mg/L.

The scope of this solute transport simulation, including the aquifer structure, boundary types, and generalization of source–sink terms, is the same as the numerical groundwater flow model. The solute transport model generalization matches the developed water flow conceptual model. Therefore, the MT3DMS solute transport model is coupled with the GMS groundwater flow model. Additionally, the simulation of solute transport prediction focuses on advection and dispersion without considering factors such as adsorption or chemical reactions. The mathematical model for solute transport is as follows:

$$\begin{cases} \frac{\partial}{\partial x}\left(D_{xx}\frac{\partial c}{\partial x}\right)+\frac{\partial}{\partial y}\left(D_{yy}\frac{\partial c}{\partial y}\right)+\frac{\partial}{\partial z}\left(D_{zz}\frac{\partial c}{\partial z}\right)-\frac{\partial(\mu_x c)}{\partial x}-\frac{\partial\left(\mu_y c\right)}{\partial y}-\frac{\partial(\mu_z c)}{\partial z}+f=\frac{\partial c}{\partial t} & (x,y,z)\in\Omega, t\geq 0 \\ c(x,y,z,0)=c_0(x,y,z) & (x,y,z)\in\Omega \\ \left(c\vec{v}-Dgradc\right)\cdot\vec{n}\Big|_{\Gamma}=\varphi(x,y,z,t) & (x,y,z)\in\Gamma, t\geq 0 \end{cases} \quad (2)$$

This equation consists of the dispersion terms in the first three terms on the left-hand side and the advection terms in the last three terms. The final term represents the increment of solute due to chemical reactions or adsorption. D_{xx}, D_{yy}, and D_{zz} are the dispersion coefficients in the x, y, and z directions; μ_x, μ_y, and μ_z are the actual water flow velocities in the x, y, and z directions; c is the solute concentration; Ω is the area of solute seepage; Γ_2 is the second type of boundary; c_0 is the initial concentration; φ is the boundary solute flux; $\vec{v}$ is the seepage velocity; gradc is the concentration gradient.

4.2. Prediction of Groundwater Pollution Impact

The impact of oily sewage on the groundwater environment of the Yunnan Anning Refinery is the most significant. Therefore, this study mainly evaluates the prediction of the impact of petroleum pollutants. Combining the stratigraphic structure and distribution of the unconfined aquifer, the locations of the wax oil hydrocracking unit and the aviation coal finished product tank area are directly covered by the unconfined aquifer on the karst aquifer without any residual or cohesive soil barrier. In the event of a leak, pollutants would penetrate the unconfined aquifer and enter the karst aquifer, causing groundwater pollution. Therefore, the wax oil hydrocracking unit and the aviation coal finished product tank area were selected for pollutant transport prediction analysis. The pollutants are conceptualized as continuous point sources, and the pollutant source is cut off as soon as the pollutant plume is detected at any monitoring well. At the initial time, the simulated concentration of the leakage source is 500 mg/L, and no adsorption, degradation, or other physical and chemical reactions are considered. Pollutant leakage mainly includes two scenarios. The first scenario is leakage from the wax oil hydrocracking unit, where pollutants leak on the surface or near the surface and then migrate in the unconfined aquifer before, after a period of time, vertically penetrating the cohesive soil weakly permeable layer to enter the sand and gravel lens. The second scenario is the simulated leakage from the aviation coal finished product tank area, where pollutants directly leak into the permeable sand and gravel lens, which is in direct contact with the karst aquifer. The locations of the two pollution sources are shown in Figure 7.

In Scenario 1, using the water quality model, a pipeline rupture or equipment leakage of petroleum pollutants to the surface or near-surface clay layer is simulated, with a leakage rate of 5.8 mL/s (0.5 m^3/d). The simulated pollutant transport results from Figure 8 show that, after 360 days of leakage, a concentration peak of 0.364 mg/L penetrates a 30 m thick unconfined aquifer and enters the Baiyunyan karst aquifer of the Yuhu Village Group. At this time, the center concentration in the clay layer is 61.193 mg/L, with a contaminated area of approximately 0.0041 km^2; the contaminated area in the sand and gravel layer is approximately 145.6 m^2. Due to the proximity of the simulated leakage point to JC22, according to Darcy's law, when pollutants enter the karst aquifer, JC22 can detect the pollutants in approximately 1 to 2 days (with a minimum concentration of approximately 0.3 mg/L).

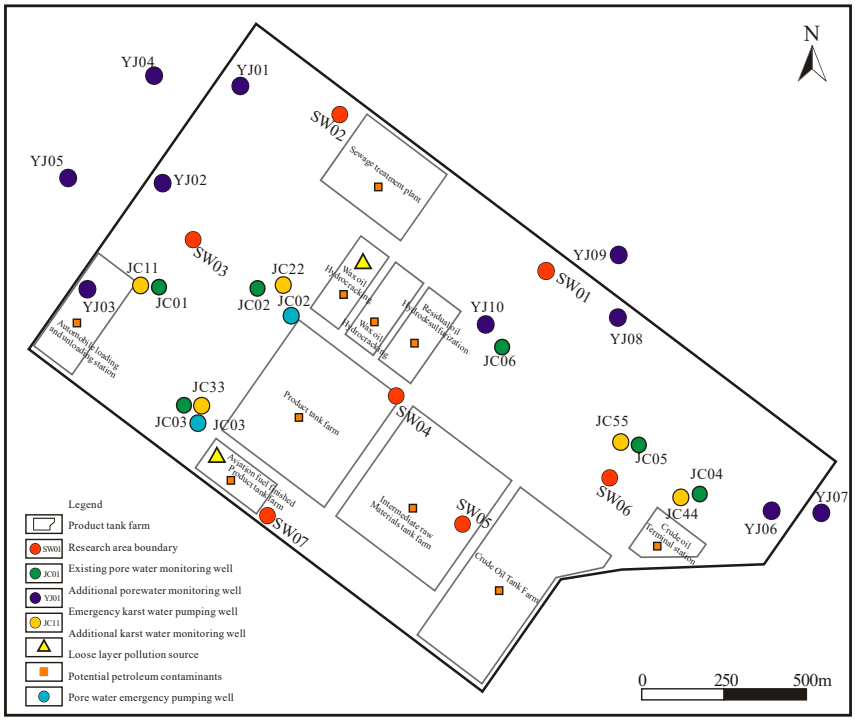

Figure 7. Pollution source location distribution map.

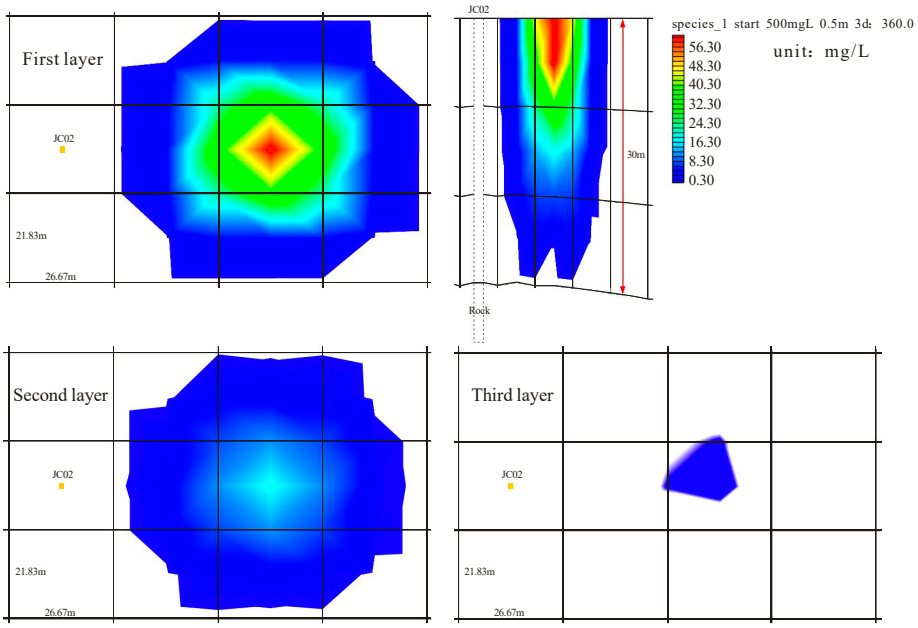

Figure 8. Contaminant plume on the 360th day in Scenario 1.

In the actual process of detecting the contaminant plume, the pollutants infiltrate vertically into the sand or gravel lens and then move horizontally with the water flow to the monitoring well from the lens. Although the horizontal permeability and dispersion coefficients of the clay are much larger than the corresponding vertical parameters, the horizontal migration distance is too long. Therefore, the transport of pollutants in the clay mainly manifests as vertical infiltration.

In Scenario 2, the water quality model is used to simulate the leakage of petroleum pollutants from underground pipelines into the sand and gravel layers. For the sake of simulation accuracy, the calculation units of the third layer of the model are refined into three layers. According to the simulation results in Figure 9, the leading edge of the

contaminant plume (30 mg/L) can penetrate the overlying unconfined aquifer and enter the underlying karst aquifer after 75 days, with a center concentration of 20.84 mg/L. According to Darcy's law, the pollutants leaking into the karst aquifer can be detected in the karst monitoring well JC33 after 1 day. However, it takes about 210 days for the leading edge of the contaminant plume (30 mg/L) to be detected in the unconfined aquifer monitoring well JC03, which is much faster than the 960 days in the clay layer (due to the weak mechanical dispersion of the clay layer overlying the sand and gravel layer, numerical dispersion occurs during the model simulation, resulting in two prominent angles in the vertical contaminant plume).

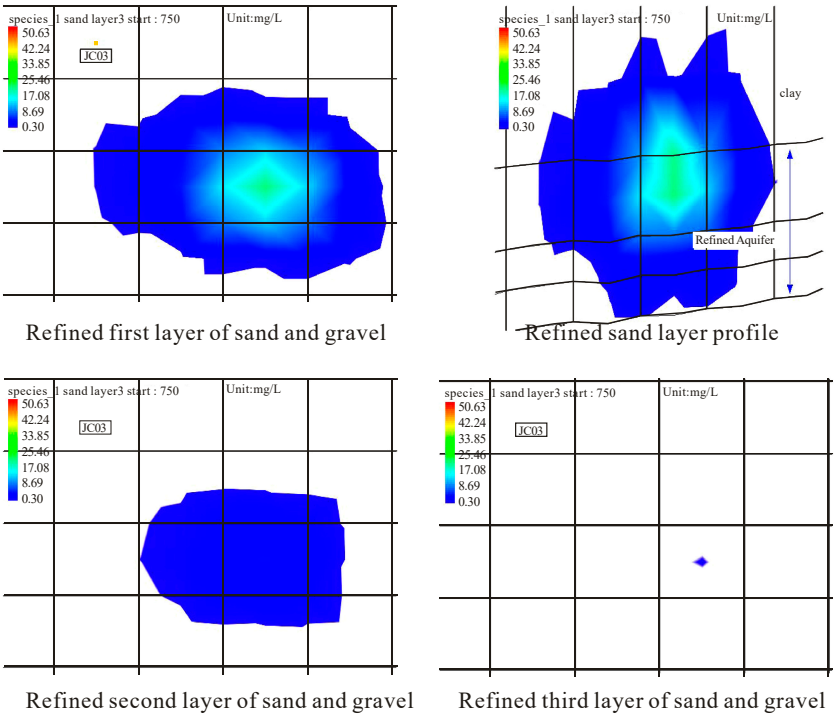

Figure 9. Scenario 2, contaminant plume at 75 days.

5. Groundwater Pollution Prevention and Control Management Research

5.1. Construction of Groundwater Pollution Prevention and Control Management Model

The most widely used method in groundwater pollution prevention and control emergency response is the extraction and treatment method. Its design and application are based on the hydrogeological conditions of the pollution area, the nature and distribution characteristics of the pollutants, and the application of groundwater hydrodynamic theory. By reasonably setting up pumping wells downstream of the pollution zone, a capture zone containing the entire groundwater pollution plume is formed. This allows for the extraction of all contaminated groundwater to achieve pollution control objectives. Pumping wells are generally located in the plume (where the hydraulic gradient is low) or downstream of the plume (where the hydraulic gradient is high). By replenishing and flushing the aquifer around or upstream of the capture zone, the concentration of pollutants in the groundwater is gradually reduced. The objective function of the pollution prevention and control model is to minimize pumping while maximizing the removal of pollutant loads from the system, ensuring that all pollutants are extracted. The model's constraint conditions mainly include karst subsidence constraints, ground subsidence constraints, and single-well pumping capacity constraints. Based on the objective function and constraint conditions, a groundwater pollution prevention and control management model for the refinery area is constructed and optimal pollutant removal schemes under different scenarios are obtained. To ensure the effective interception of the pollution plume, when pollutants are detected in monitoring wells, the information is fed back to the control system and emergency wells,

and monitoring wells should be activated promptly. Therefore, the duration, quantity, and pumping rates of emergency and monitoring wells (i.e., the total pumping volume of emergency wells in a certain management period) are the decision variables of this system. Considering the objective function, various constraint conditions and decision variables, the pollution prevention and control management model for the groundwater system of the Anning Refinery is:

$$\begin{cases} Minz = \sum_{j=1}^{m} \sum_{i=1}^{n} C_{(j,i)} Q_{(j,i)} \\ \sum M = \sum M' \end{cases} \tag{3}$$

$$S.T. \begin{cases} Q_{(j,i)} \leq q_{(j,i)} \\ \{H_l\} \leq \{H\}_k \leq \{H_u\} \\ \{W_l\} \leq \{W\}_k \leq \{W_u\} \\ T \leq T' \\ S \leq S' \\ j = 1, 2 \cdots, 5 \\ i = 1 \end{cases} \tag{4}$$

The interpolation method used in the numerical simulation involves finite difference. Therefore, the equations of a series of constraints in the study area, along with the hydrological and water quality models, are combined and solved using the numerical model. Various operational conditions designed for the study area are considered, and a series of constraints are incorporated into the numerical model, along with the hydrological and solute transport models, to solve for the most effective pollution control measures under different conditions. When dealing with pollution through pumping, the pumping wells are set up as concentration observation wells at the same time the solute transport model is used. This allows for monitoring the relationship between the pollutant concentrations in various observation wells and at various times under different pumping rates, as well as selecting the optimal pumping scheme based on data analysis. Emergency disposal wells are activated to treat oil pollution. Under pumping conditions, when the flow rate reaches a certain value, a cone of depression forms, increasing the groundwater flow velocity and hydraulic gradient. As a result, pollutants flow back towards the pumping well, leading to an increase in pollutant concentration near the pumping well. The greater the pumping rate, the faster the pollutants flow back; a greater inward hydraulic gradient is also formed, which improves the efficiency of pollutant control. However, excessive pumping can lead to the groundwater recharge rate in the aquifer being lower than the pumping rate, resulting in the aquifer being dewatered, affecting downstream wells and spring water levels and causing some geological hazards. Therefore, it is necessary to provide a reasonable pumping scheme based on different operational conditions to control pollutants with the minimum pumping volume. When pollutants are detected to be leaking in monitoring wells, emergency disposal wells are immediately activated, and monitoring wells can also be used as emergency disposal wells if necessary. The cone of depression must completely envelop the plume to ensure that all leaked pollutants are pumped out and treated. Using numerical models to estimate the time required for all pollutants to reach the pumping well, which serves as a basis for the pumping duration. Pumping can only be stopped when the sample tests meet the standards.

5.2. Groundwater Pollution Control Plan

Based on the geological structure, the local area of the plant is directly in contact with the karst aquifer, and once pollutants leak, they will pose a threat to the karst aquifer. Pollutants may leak in two locations, either on the surface or in the near-surface clay layer or directly into the sand and gravel lenses, so two scenarios are simulated. Scenario 1 is that pollutants leak on the surface or near the surface, then migrate through the unconfined aquifer and, after a period of time, vertically penetrate the clay weak aquifer, enter the sand and gravel lenses, and finally enter the karst aquifer in the form of long-term low concentrations. Scenario 2 is that pollutants leak directly into the permeable sand and

gravel lenses. The residence time of pollutants in the unconfined aquifer is relatively short and the concentration entering the karst aquifer is relatively high.

Scenario 1: When pollutants leak for 360 days, monitoring well JC22 detects the pollution plume. Assuming that measures are taken immediately to cut off the pollution source and activate JC02, the pumping duration should not exceed 207 days due to the ground subsidence constraint. The maximum pumping rate is 26 m^3/d based on the pumping well's pumping capacity constraint. Pumping is conducted to meet all constraints. When JC02 has been pumping for 205 days, the center concentration of the pollution plume decreases from 61.93 mg/L to 52.216 mg/L. The lowest concentration in the sand and gravel lenses plume is 0.36 mg/L. Horizontally, the pollution plume moves slowly towards pumping well JC02, with a slight decrease in the center concentration of pollutants. Vertically, pollutants continue to leak (Figure 10 and Table 3).

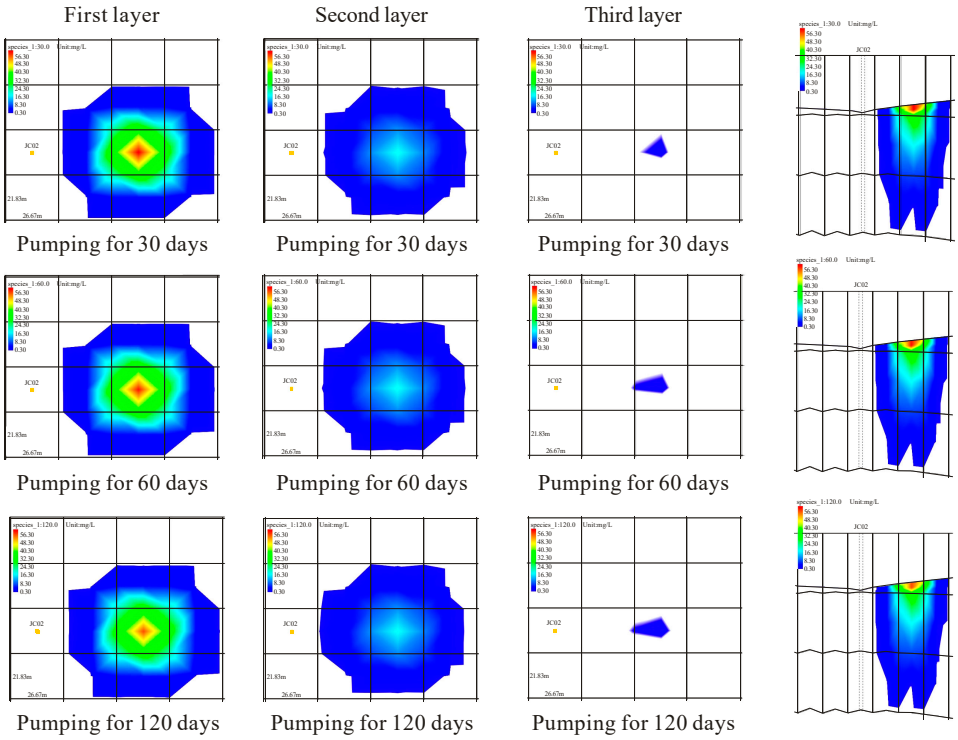

Figure 10. Migration of the pollution plume under continuous pumping conditions at JC02.

Table 3. Center concentration values of each layer under pumping conditions at JC02.

Duration of Pumping Center / Concentration Value	30	60	120
First layer:	59.77	58.39	55.73
Second layer:	17.04	17	16.91
Third layer:	0.336	0.333	0.34

The simulation results indicate that the clay layer has a good pollution isolation capability, with a slow horizontal diffusion of pollutants in the clay layer. It takes a long time for pollutants to be detected in the monitoring wells in the unconfined aquifer. At this time, the low-concentration pollution plume may have already penetrated the unconfined aquifer and entered the underlying karst aquifer. Because the concentration of pollutants entering the karst aquifer is low, pollutants can only be detected in karst water monitoring wells close to the leakage point. If the karst water monitoring wells are far from the leakage point, the dilution effect of karst water may reduce the pollutant concentration below the detection limit, making it undetectable. Initiating pumping at well JC02 can help mitigate

the downward infiltration of pollutants to some extent. Since pumping has little effect on reducing the concentration value, it is recommended to immediately start well JC22 after discovering pollutant leakage while simultaneously starting the unconfined aquifer monitoring wells at a fixed frequency and pumping at maximum pumping capacity (Figure 11).

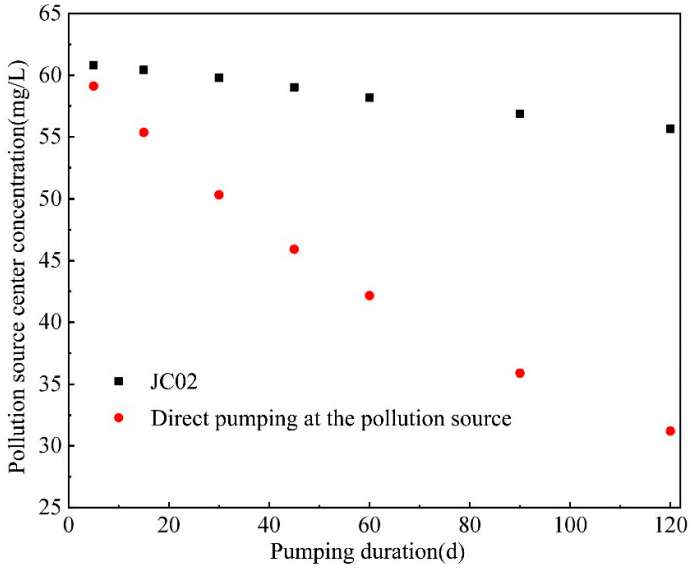

Figure 11. Trend chart of the center concentration of pollutants at the pollution source when pumping directly from JC02.

Assuming that petroleum pollutants leak from the surface, the pollutants need to slowly penetrate the clay layer before the low-concentration front of the pollution plume can reach the aquifer (gravel and sand). The groundwater entering the monitoring wells or emergency wells mainly comes from the gravel lens and sand lens. Pumping from monitoring wells or emergency wells near the pollution source can only extract pollutants with lower concentrations, resulting in very little pollutant mass being pumped out. Therefore, long-term pumping has little effect on reducing the center concentration of the pollution plume. If the monitoring wells or emergency wells are very close to the pollution source (assumed to be directly at the pollution source in the model), although the permeability coefficient of the clay layer is poor, the water flow extracted from the underlying gravel lens and sand lens can carry out a large amount of pollutants, and the efficiency and effectiveness of pollution prevention are significantly better than using nearby monitoring wells. Continuous pumping for 120 days from nearby monitoring wells only reduces the center concentration of the pollution source by 8.6%, while pumping directly at the pollution source reduces the center concentration by 47.3% (Figures 12 and 13). Therefore, it is recommended to place monitoring wells as close to the potential pollution source as possible, and the monitoring wells should penetrate the gravel or sand lens. Due to the poor mechanical dispersion ability of the clay, numerical dispersion may occur during solute transport simulation, as shown in Figure 12. When pumping at the center of the pollution source, as the simulation time progresses, the surrounding low-concentration pollution plume expands outward.

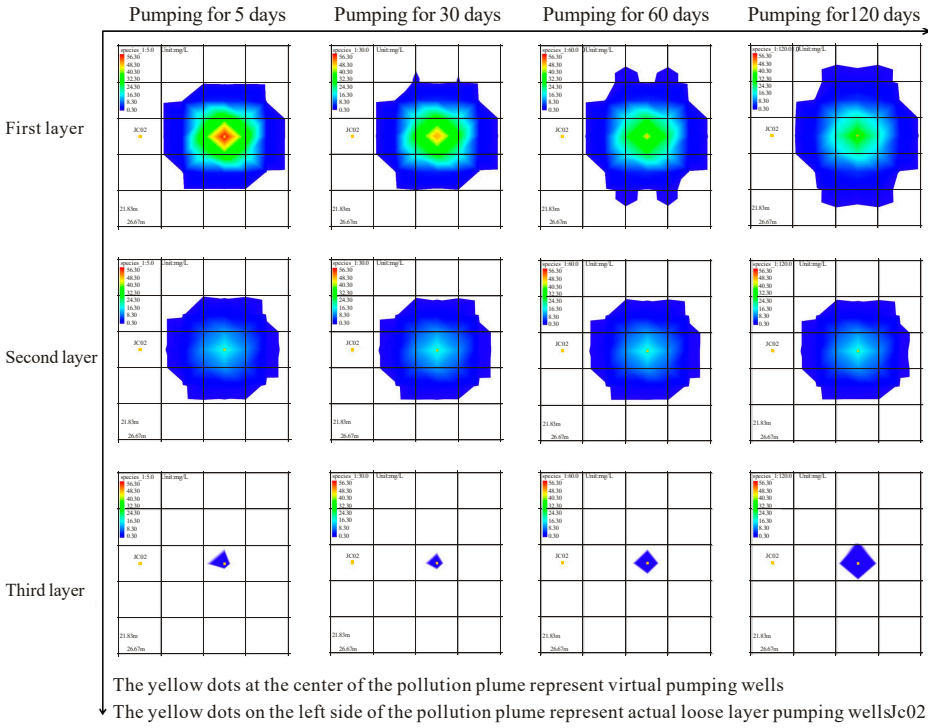

Figure 12. The movement of the pollution plume under continuous pumping conditions at the pollution source.

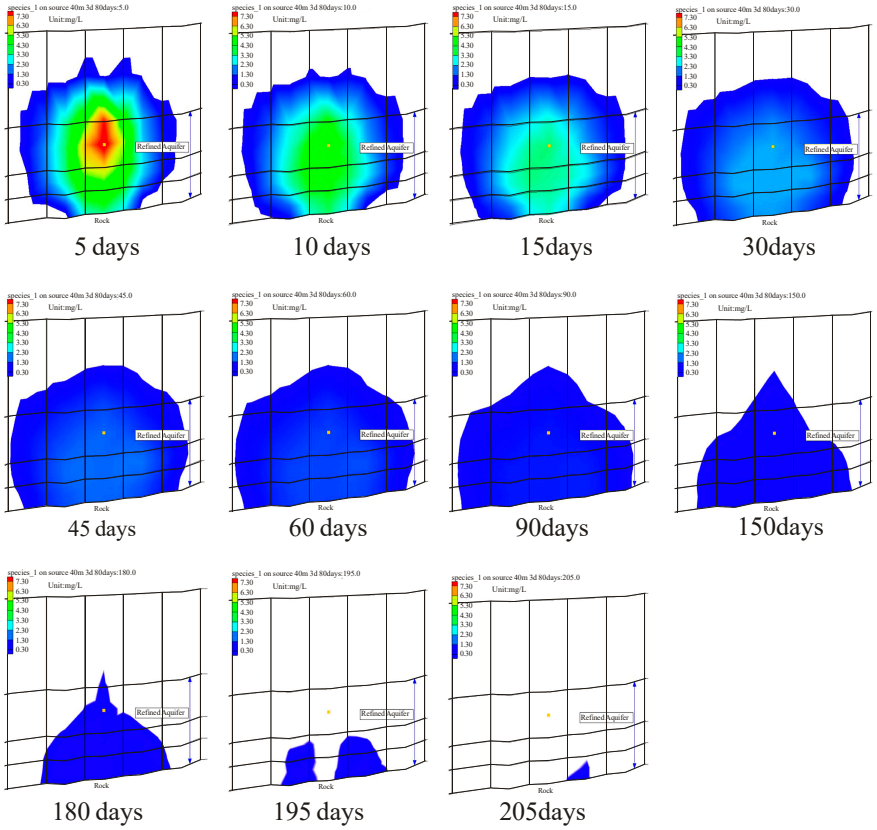

Figure 13. Migration of the pollution plume under continuous pumping conditions at JC03.

In Scenario 1, after the pollutant leaks, it lingers for a long time in the backfill soil and clay layer, with the specific duration being closely related to the thickness of the backfill soil and clay layer at the leak site. The movement of the pollutant in the clay is slow both horizontally and vertically. Compared to horizontal movement, vertical movement is much shorter, so the pollutant mainly moves vertically downward. When the pollutant enters the sand and gravel aquifer, it starts to horizontally disperse with the relatively fast groundwater flow. However, since some sand and gravel aquifers are directly in contact with the underlying karst aquifer, the low-concentration plume (0.3 mg/L) penetrates the sand and gravel aquifers in a shorter time than it would take to move horizontally to downstream of the unconsolidated aquifer monitoring wells. Therefore, the pollutant has entered the karst aquifer before being detected in the unconsolidated aquifer monitoring wells. The pollutant migrates downstream quickly with the fast-flowing karst water and, generally, the pollution is detected earlier in karst water monitoring wells than in unconsolidated aquifer monitoring wells. Due to the interception effect of the clay layer, high-concentration pollutants remain in the clay for a long time, and only low-concentration pollutants continuously enter the sand and gravel aquifers and then the karst aquifer, with the pollutant concentration in the aquifers being slightly higher than in the karst aquifer.

When a low-concentration plume is detected in karst water monitoring wells, it indicates that the overlying unconsolidated aquifer has been contaminated with a higher concentration of pollutants. At this point, it is necessary to immediately activate the karst water monitoring wells or emergency wells to intercept the low-concentration pollutants infiltrating from the unconsolidated aquifer and simultaneously search for the pollution source. Activating the nearest unconsolidated aquifer monitoring wells or emergency wells to the pollution source ensures the maximum control of the infiltrating pollutant concentration. The closer the well is to the pollution source, the higher the pumping efficiency and the faster the reduction in the center concentration of the pollution plume, provided that the monitoring wells or emergency wells expose the sand and gravel aquifers. If the area around the pollutant leak consists entirely of clay and lacks aquifers, the effectiveness of pumping wells may be limited. The natural recharge conditions of the unconsolidated aquifer in the factory area may be poor and may not be able to sustain prolonged pumping. Therefore, it may be necessary to use intermittent pumping to control the infiltration of pollutants after their discovery, depending on the actual conditions. In this case, if only karst water monitoring wells and unconsolidated aquifer monitoring wells are used for pumping to control the migration of pollutants, it may be difficult to completely remove the pollutants retained in the clay layer in the short term.

Scenario 2: Assuming that the pollution plume penetrates vertically through the unconsolidated aquifer into the karst aquifer and is detected, immediate measures are taken to discover and intercept the pollution source within a few days. The concentration distribution of pollutants at day 80 is taken as the initial concentration for the pumping stage. Pumping at a rate of 40 m^3/d from JC03, only 1.03% of the pollutants can be pumped out in 205 days (the maximum continuous pumping duration due to ground subsidence is 207 days). Even if pumping is carried out at the same rate directly from the pollution source, only 9.0% of the pollutants can be removed. As shown in Figure 13 the main part of the pollution plume is not reduced by pumping from the well but rather seeps into the karst aquifer of Yuhu Village Group along with groundwater flow from the higher hydraulic head sand or gravel aquifers to the lower hydraulic head. Therefore, if the pollution directly occurs in the sand or gravel aquifers that directly contact the karst aquifer, due to the characteristics of the unconsolidated aquifer and the limitations of the pumping capacity of the unconsolidated aquifer monitoring wells, using the unconsolidated aquifer monitoring wells for pollution control is not very effective. It is recommended to use the nearest karst aquifer monitoring wells or emergency wells for pollution control.

In Scenario 2, the pollutants do not need to penetrate the clay layer, and the horizontal and vertical migration times of pollutants in the sand and gravel lenses are relatively shorter than in Scenario 1. Although the permeability of the sand and gravel lenses is good, similar

to the clay layer, the vertical migration distance of pollutants in them is much smaller than the horizontal movement distance, so vertical migration is still predominant. Compared to Scenario 1, pollutants can quickly enter the underlying karst aquifer in Scenario 2, with a relatively high percolation concentration ranging from 1 to 102 mg/L under the current simulation conditions. Similarly, although the horizontal migration speed of pollutants in the sand and gravel lenses is much faster than in the clay layer, it is still slower than in the karst water, so once the unconfined aquifer is penetrated, pollutants are more likely to be detected in downstream karst water monitoring wells. Numerical simulations have found that, even in Scenario 2, opening a pumping well in the unconfined aquifer directly at the source of pollution still makes it difficult to control the infiltration of pollutants. This is because the allowable pumping volume of the unconfined aquifer is small and it is difficult to capture all the pollution plumes with the formed funnel. Therefore, if high concentrations of pollutants are found in karst water monitoring wells, it is recommended to mainly use karst water monitoring wells for prevention and control, as the use of unconfined aquifer monitoring wells is not very helpful. In this case, once the pollution source is cut off, pollutants in the sand and gravel lenses generally enter the karst aquifer completely within a year, unlike pollutants in the clay layer, which may remain for a long time. As long as the pumping activity of downstream karst water monitoring wells is maintained, it is possible to intercept and control the infiltration of pollutants.

6. Conclusions

This article focuses on the groundwater of the Anning Refinery in Yunnan Province. By coupling a numerical simulation of groundwater flow with the construction of a groundwater pollution transport model, a groundwater pollution prevention and control management model was developed. It deeply explores the transport laws of pollution plumes under different pollution scenarios and proposes a multi-objective groundwater pollution control scheme. The main conclusions are as follows:

1. A numerical groundwater flow model was constructed using the MODFLOW module in GMS software. Under natural flow field conditions and the conditions of a group of well pumping tests, the groundwater flow model fit well, with small errors, showing a trend in flow from south to north.
2. On the basis of the GMS groundwater flow model, a groundwater solute transport model was developed by coupling with the MT3DMS model. The dispersion data measured by a sodium chloride tracer were used to calibrate the model, and a pollution transport prediction analysis of two potential pollution sources, the wax hydrocracking unit and the aviation coal finished product tank area, was conducted. In Scenario 1, when petroleum pollutants enter the karst aquifer, the nearby karst monitoring wells can detect them in about 1–2 days. In Scenario 2, petroleum pollutants in the karst aquifer can be detected in karst monitoring wells after 1 day.
3. Combining constraints such as karst collapse, ground subsidence, and single-well water output capacity in the study area, a groundwater pollution prevention and control management model was constructed to simulate optimal removal schemes for groundwater pollutants under different scenarios. In Scenario 1, when a low-concentration pollution plume is detected in the karst water monitoring wells, it indicates that the upstream unconfined aquifer has been subjected to a high concentration of pollution and the nearest unconfined aquifer and karst water monitoring wells or emergency wells should be opened immediately. In Scenario 2, when a low-concentration pollution plume is detected in the karst water monitoring wells, the efficiency of using the unconfined aquifer monitoring wells for drainage is low, so the nearest karst water monitoring wells or emergency wells should be used for pollution prevention and control.

The findings emphasize the importance of proactive monitoring and emergency response measures tailored to the specific hydrogeological conditions of the region, validate the value of coupled numerical modeling approaches in simulating pollutant migration,

and provide a framework for assessing the efficacy of different pollution control scenarios. Overall, the study has important implications for the management and protection of groundwater resources and guides the development of more effective management strategies in industrial areas, especially in areas with high pollution risks, with a view to providing new ideas and insights for the provision of similar industrial environments worldwide.

Author Contributions: Conceptualization, X.F. and S.T.; Methodology, Z.N.; Software, J.T.; Validation, J.T. and Z.N.; Formal analysis, X.F.; Investigation, J.T. and Z.N.; Resources, S.T.; Data curation, Z.N.; Writing—original draft, Z.N.; Writing—review and editing, J.T.; Visualization, X.F. and S.T.; Supervision, X.F. and X.F.; Project administration, S.T.; Funding acquisition, S.T. All authors have read and agreed to the published version of the manuscript.

Funding: This research was supported by the "Unveiling and Leading" project (No. 202303) of the China Natural Uranium Technology Innovation Consortium, which was provided by the China Nuclear Uranium Co., Ltd.

Data Availability Statement: The data presented in this study are available on request from the authors.

Acknowledgments: We thank Petrochina Yunnan Petrochemical Co., Ltd. for providing the groundwater data for this work. The authors are also grateful to the editor and reviewers for providing valuable comments and suggestions for this article.

Conflicts of Interest: The authors declare no conflicts of interest.

References

1. Wu, J.; Bian, J.; Wan, H.; Ma, Y.; Sun, X. Health risk assessment of groundwater nitrogen pollution in Songnen Plain. *Ecotoxicol. Environ. Saf.* **2020**, *207*, 111245. [CrossRef] [PubMed]
2. Jasechko, S.; Perrone, D. Global groundwater wells at risk of running dry. *Science* **2021**, *372*, 418–421. [CrossRef] [PubMed]
3. Hartmann, A.; Jasechko, S.; Gleeson, T.; Wada, Y.; Andreo, B.; Barbera, J.A.; Brielmann, H.; Bouchaou, L.; Charlier, J.; Darling, W.G.; et al. Risk of groundwater contamination widely underestimated because of fast flow into aquifers. *Proc. Natl. Acad. Sci. USA* **2021**, *118*, e2024492118. [CrossRef] [PubMed]
4. Yang, N.; Winkel, L.H.E.; Johannesson, K.H. Predicting geogenic arsenic contamination in shallow groundwater of south Louisiana, United States. *Environ. Sci. Technol.* **2014**, *48*, 5660–5666. [CrossRef]
5. Adimalla, N. Groundwater Quality for Drinking and Irrigation Purposes and Potential Health Risks Assessment: A Case Study from Semi-Arid Region of South India. *Expo. Health* **2018**, *11*, 109–123. [CrossRef]
6. Braunig, J.; Baduel, C.; Heffernan, A.; Rotander, A.; Donaldson, E.; Mueller, J.F. Fate and redistribution of perfluoroalkyl acids through AFFF-impacted groundwater. *Sci. Total Environ.* **2017**, *596*, 360–368. [CrossRef]
7. Li, X.; Jiao, W.; Xiao, R.; Chen, W.; Liu, W. Contaminated sites in China: Countermeasures of provincial governments. *J. Clean. Prod.* **2017**, *147*, 485–496. [CrossRef]
8. Guo, Y.; Li, P.; He, X.; Wang, L. Groundwater Quality in and Around a Landfill in Northwest China: Characteristic Pollutant Identification, Health Risk Assessment, and Controlling Factor Analysis. *Expo. Health* **2022**, *14*, 885–901. [CrossRef]
9. Chen, R.; Teng, Y.; Chen, H.; Hu, B.; Yue, W. Groundwater pollution and risk assessment based on source apportionment in a typical cold agricultural region in Northeastern China. *Sci. Total Environ.* **2019**, *696*, 133972. [CrossRef]
10. Zhao, Y.; Lin, L.; Hong, M. Nitrobenzene contamination of groundwater in a petrochemical industry site. *Front. Environ. Sci. Eng.* **2019**, *13*, 29. [CrossRef]
11. Maldaner, C.H.; Munn, J.D.; Coleman, T.; Molson, J.M.; Parker, B.L. Groundwater Flow Quantification in Fractured Rock Boreholes Using Active Distritbuted Temperature Sensing Under Natural Gradient Conditions. *Water Res.* **2019**, *55*, 3285–3306. [CrossRef]
12. Burri, N.M.; Weatherl, R.; Moeck, C.; Schirmer, M. A review of threats to groundwater quality in the Anthropocene. *Sci. Total Environ.* **2019**, *684*, 136–154. [CrossRef] [PubMed]
13. Skurray, J.H.; Roberts, E.J.; Pannell, D.J. Hydrological challenges to groundwater trading:Lessons from south-west Western Australia. *Hydrogeol. J.* **2013**, *412*, 256–268.
14. Shu, S.; Zhu, W.; Shi, J. A new simplified method to calculate breakthrough time of municipal solid waste landfill liners. *J. Clean. Prod.* **2019**, *219*, 649–654. [CrossRef]
15. Li, J.; Yang, Y.; Huan, H.; Li, M.; Xi, B.; Lv, N.; Wu, Y.; Xie, Y.; Li, X.; Yang, J. Method for screening prevention and control measures and technologies based on groundwater pollution intensity assessment. *Sci. Total Environ.* **2016**, *551*, 143–154. [CrossRef]
16. Wang, Y.; Geng, F.; Yang, S.; Jing, H.; Meng, B. Numerical simulation of particle migration from crushed sandstones during groundwater inrush. *J. Hazard. Mater.* **2018**, *362*, 327–335. [CrossRef]
17. Hosono, T.; Wang, C.; Umezawa, Y.; Nakano, T.; Onodera, S.; Nagata, T.; Yoshimizu, C.; Tayasu, I.; Taniguchi, M. Multiple isotope (H, O, N, S and Sr) approach elucidates complex pollution causes in the shallow groundwaters of the Taipei urban area. *Hydrogeol. J.* **2011**, *397*, 23–36. [CrossRef]

18. Matiatos, I. Nitrate source identification in groundwater of multiple land-use areas by combining isotopes and multivariate statistical analysis: A case study of Asopos basin (Central Greece). *Sci. Total Environ.* **2016**, *541*, 802–814. [CrossRef] [PubMed]
19. Azzellino, A.; Colombo, L.; Lombi, S.; Marchesi, A.; Piana, A.; Andrea, M.; Alberti, L. Groundwater diffuse pollution in functional urban areas: The need to define anthropogenic diffuse pollution background levels. *Sci. Total Environ.* **2019**, *656*, 1207–1222. [CrossRef]
20. Wu, H.; Dong, Y.; Gao, L.; Song, X.; Liu, F.; Peng, X.; Zhang, G. Identifying Nitrate Sources in Surface Water, Regolith and Groundwater in a Subtropical Red Soil Critical Zone by Using Dual Nitrate Isotopes. *Catena* **2021**, *198*, 104994. [CrossRef]
21. Naderi, M.; Jahanshahi, R.; Dehbandi, R. Two distinct mechanisms of fluoride enrichment and associated health risk in springs' water near an inactive volcano, southeast Iran. *Ecotoxicol. Environ. Saf.* **2020**, *195*, 110503. [CrossRef] [PubMed]
22. Shao, S.; Yang, X.; Jia, C. Combining multi-source data to evaluate the leakage pollution and remediation effects of landfill. *Hydrogeol. J.* **2022**, *610*, 127889. [CrossRef]
23. Buckerfield, S.J.; Quilliam, R.S.; Bussiere, L.; Waldron, S.; Naylor, L.A.; Li, S.; Oliver, D.M. Chronic urban hotspots and agricultural drainage drive microbial pollution of karst water resources in rural developing regions. *Sci. Total Environ.* **2020**, *744*, 140898. [CrossRef] [PubMed]
24. Qi, S.; Luo, J.; O'Connor, D.; Cao, X.; Hou, D. Influence of groundwater table fluctuation on the non-equilibrium transport of volatile organic contaminants in the vadose zone. *Hydrogeol. J.* **2020**, *580*, 124353. [CrossRef]
25. Guo, Z.; Brusseau, M.L.; Fogg, G.E. Determining the long-term operational performance of pump and treat and the possibility of closure for a large TCE plume. *Hazard. Mater. J.* **2019**, *365*, 796–803. [CrossRef]
26. Liolios, K.; Moutsopoulos, K.N.; Tsihrintzis, V.A. Modeling of flow and BOD fate in horizontal subsurface flow constructed wetlands. *Chem. Eng. J.* **2012**, *200*, 681–693. [CrossRef]
27. Chang, S.; Clement, T.; Simpson, M.J.; Lee, K. Does sea-level rise have an impact on saltwater intrusion. *Adv. Water Res.* **2011**, *34*, 1283–1291. [CrossRef]
28. Xiao, H.; Wang, D.; Medeiros, S.C.; Hagen, S.C.; Hall, C.R. Assessing sea-level rise impact on saltwater intrusion into the root zone of a geo-typical area in coastal east-central Florida. *Sci. Total Environ.* **2018**, *630*, 211–221. [CrossRef]
29. Sreekanth, J.; Datta, B. Coupled simulation-optimization model for coastal aquifer management using genetic programming-based ensemble surrogate models and multiple-realization optimization. *Water Res.* **2011**, *47*, W04516. [CrossRef]
30. Liu, Y.; Ao, C.; Zeng, W.; Srivastava, A.K.; Gaiser, T.; Wu, J.; Huang, J. Simulating water and salt transport in subsurface pipe drainage systems with HYDRUS-2D. *Hydrogeol. J.* **2021**, *592*, 125823. [CrossRef]
31. Ahmed, I.I.K.; Fea, A.; Au, L.; Ang, R.E.; Harasymowycz, P.; Jampel, H.; Samuelson, T.W.; Chang, D.F.; Rhee, D.J. A prospective randomized trial comparing Hydrus and iStent micro-invasive glaucoma glaucoma surgery implants for standalone treatment of open-angle glaucoma: The COMPARE Study. *Ophthalmology* **2020**, *127*, 52–61. [CrossRef]
32. Chen, N.; Li, X.; Simunek, J.; Shi, H.; Hu, Q.; Zhang, Y. Evaluating soil nitrate dynamics in an intercropping dripped ecosystem using HYDRUS-2D. *Sci. Total Environ.* **2020**, *718*, 137314. [CrossRef] [PubMed]
33. Li, J.; Zhao, R.; Li, Y.; Li, H. Simulation and optimization of layered bioretention facilities by HYDRUS-1D model and response surface methodology. *Hydrogeol. J.* **2020**, *586*, 124813. [CrossRef]
34. Zhou, P.; Wang, G.; Duan, R. Impacts of Long-Term Climate Change on The Groundwater Flow Dynamics in A Regional Groundwater System: Case Modeling Study in Alashan, China. *Hydrogeol. J.* **2020**, *590*, 125557. [CrossRef]
35. Tabelin, C.B.; Uyama, A.; Tomiyama, S.; Villacorte-Tabelin, M.; Phengsaart, T.; Silwamba, M.; Jeon, S.; Park, I.; Arima, T.; Igarashi, T. Geochemical audit of a historical tailings storage facility in Japan: Acid mine drainage formation, zinc migration and mitigation strategies. *J. Hazard. Mater.* **2022**, *438*, 129453. [CrossRef]
36. Vu, T.; Ni, C.; Li, W.; Truong, M.; Hsu, S.M. Predictions of groundwater vulnerability and susta-inability by an integrated index-overlay method and physical-based numerical model. *Hydrogeol. J.* **2021**, *596*, 126082.
37. Morway, E.; Niswonger, R.; Langevin, C.; Bailey, R.; Healy, R. Modeling variably saturated subsurface solute transport with MODFLOW-UZF and MT3DMS. *Groundwater* **2013**, *51*, 237–251. [CrossRef]
38. Beegum, S.; Šimůnek, J.; Szymkiewicz, A.; Sudheer, K.; Nambi, I. Implementation of Solute Transport in the Vadose Zone into the 'HYDRUS Package for MODFLOW'. *Groundwater* **2019**, *57*, 392–408. [CrossRef]
39. Mao, W.; Zhu, Y.; Ye, M.; Zhang, X.; Wu, J.; Yang, J. A new quasi-3-D model with a dual iterative coupling scheme for simulating unsaturated-saturated water flow and solute transport at a regional scale. *Hydrogeol. J.* **2021**, *602*, 12. [CrossRef]
40. Graaf, I.I.E.M.D.; Gleeson, T.; Beek, L.P.H.; Sutanudjaja, E.H.; Bierkens, M.F.P. Envir-onmental flow limits to global groundwater pumping. *Nature* **2019**, *574*, 7776. [CrossRef]
41. Yao, N.; Li, C.; Yu, J.; Xu, Q.; Wei, S.; Tian, Z.; Yang, Z.; Yang, W.; Shen, J. Insight into adsorption of combined antibiotic-heavy metal contaminants on graphene oxide in water. *Sep. Purif. Technol.* **2020**, *236*, 116278. [CrossRef]
42. Sousa, J.C.G.; Ribeiro, A.R.; Barbosa, M.O.; Pereira, M.F.R.; Silva, A.M.T. A review on environmental monitoring of water organic pollutants identified by EU guidelines. *J. Hazard. Mater.* **2018**, *344*, 146–162. [CrossRef] [PubMed]
43. Ani, I.J.; Akpan, U.G.; Olutoye, M.A.; Hameed, B.H. Photocatalytic degradation of pollutants in petroleum refinery wastewater by TiO_2 and ZnO-based photocatalysts: Recent development. *Clean. Prod. J.* **2018**, *205*, 930–954. [CrossRef]
44. Elshall, A.S.; Ye, M.; Finkel, M. Evaluating Two Multi-Model Simulation-Optimization Approaches for Managing Groundwater Contaminant Plumes. *Hydrogeol. J.* **2020**, *590*, 125427. [CrossRef]

45. Mao, L.; Revil, A.; Hort, R.D.; Munakatamarr, J.; Atekwana, E.A.; Kulessa, B. Resistivity and self-potential tomography applied to groundwater remediation and contaminant plumes: Sandbox and field experiments. *Hydrogeol. J.* **2015**, *530*, 1–14. [CrossRef]
46. Morrissy, J.G.; Currell, M.J.; Reichman, S.M.; Surapaneni, A.; Megharaj, M.; Crosbie, N.D.; Hirth, D.; Aquilina, S.; Rajendram, W.; Ball, A.S. Nitrogen Contamination and Bioremediation in Groundwater and The Environment: A Review. *Earth-Sci. Rev.* **2021**, *222*, 103816. [CrossRef]